Research

New Phytologist

# Genetic control of photoprotection and photosystem II operating efficiency in plants

**Seema Sahay[1,2]*, Marcin Grzybowski[2,3,4]*, James C. Schnable[2,3] and Katarzyna Głowacka[1,2,5]**

[1]Department of Biochemistry, Beadle Center, University of Nebraska-Lincoln, Lincoln, NE 68588, USA; [2]Center for Plant Science Innovation, University of Nebraska-Lincoln, Lincoln, NE 68588, USA; [3]Department of Agronomy and Horticulture, University of Nebraska-Lincoln, Lincoln, NE 68583, USA; [4]Department of Plant Molecular Ecophysiology, Faculty of Biology, Institute of Plant Experimental Biology and Biotechnology, University of Warsaw, 02-096 Warsaw, Poland; [5]Institute of Plant Genetics, Polish Academy of Sciences, 60-479 Poznań, Poland

Author for correspondence:
*Katarzyna Glowacka*
*Email: kglowacka2@unl.edu*

Received: *7 December 2022*
Accepted: *22 April 2023*

*New Phytologist* (2023) **239:** 1068–1082
**doi**: 10.1111/nph.18980

**Key words:** GWAS, natural genetic variations, nonphotochemical quenching, photosynthesis, photosystem II operating efficiency, *Zea mays*.

## Summary

- Photoprotection against excess light via nonphotochemical quenching (NPQ) is indispensable for plant survival. However, slow NPQ relaxation under low light conditions can decrease yield of field-grown crops up to 40%.
- Using semi-high-throughput assay, we quantified the kinetics of NPQ and photosystem II operating efficiency (ΦPSII) in a replicated field trial of more than 700 maize (*Zea mays*) genotypes across 2 yr. Parametrized kinetics data were used to conduct genome-wide association studies.
- For six candidate genes involved in NPQ and ΦPSII kinetics in maize the loss of function alleles of orthologous genes in Arabidopsis (*Arabidopsis thaliana*) were characterized: two thioredoxin genes, and genes encoding a transporter in the chloroplast envelope, an initiator of chloroplast movement, a putative regulator of cell elongation and stomatal patterning, and a protein involved in plant energy homeostasis.
- Since maize and Arabidopsis are distantly related, we propose that genes involved in photoprotection and PSII function are conserved across vascular plants. The genes and naturally occurring functional alleles identified here considerably expand the toolbox to achieving a sustainable increase in crop productivity.

## Introduction

Despite continuous improvements, the pace with which the yield of staple crops is currently increasing is not sufficient to prevent food shortages by 2050 (Ray *et al.*, 2012). Furthermore, achieving food security will require mitigating or compensating for yield losses caused by intensifying adverse environmental conditions, such as late-spring or early-fall cold spells, heat, drought, and reduced soil fertility, individually or in combination (Lobell *et al.*, 2014; Dalin *et al.*, 2017; Kim *et al.*, 2017; Zhao *et al.*, 2017). The primary engine of plant productivity is photosynthesis. Model simulations and proof-of-concept studies show that yield can be improved by enhancing photosynthetic efficiency (Zhu *et al.*, 2004; Kromdijk *et al.*, 2016; Köhler *et al.*, 2017; South *et al.*, 2019; López-Calcagno *et al.*, 2020; De Souza *et al.*, 2022). Here, we identified candidate genes in maize (*Zea mays*) involved in the dynamic control of light harvesting in photosynthesis and verified their orthologs in Arabidopsis (*Arabidopsis thaliana*), which could be used to improve photosynthesis in crops grown under field conditions.

Crops growing in the field have to cope with frequent, rapid, and irregular changes in natural light conditions, even on cloud-free days, as a result of changes in the position of the sun, movement of leaves, self-shading, and shading from neighboring plants (Zhu *et al.*, 2004; Burgess *et al.*, 2016). When more light is absorbed than can be utilized by photochemistry, the overexcitation of antennae associated with photosystem II (PSII) can lead to the formation of reactive oxygen species, photooxidation, and photodamage (Müller *et al.*, 2001). A prevalent and ubiquitous photoprotective mechanism harmlessly dissipates excess excitation energy as heat, called nonphotochemical quenching of chlorophyll fluorescence (NPQ). While NPQ is critical to protecting the photosynthetic apparatus (Roach & Krieger-Liszkay, 2012), the slow rate of relaxation of NPQ during the transition from saturated to limited light conditions reduces PSII operating efficiency (ΦPSII) and $CO_2$ fixation (Hubbart *et al.*, 2012; Kromdijk *et al.*, 2016). Accelerating NPQ decay (relaxation) via a transgenic approach resulted in a significant gain (22%) in photosynthesis and yield (Kromdijk *et al.*, 2016) and model simulations predict that this approach can improve yield by up to 35% (Zhu *et al.*, 2004).

Despite intensive studies on NPQ, the site and mechanism of NPQ are not resolved (Demmig-Adams *et al.*, 2014; Ruban & Wilson, 2021). For NPQ to occur, photosynthetic antennae need to switch from funneling energy to the reaction center to dispersing excess energy. This requires conformational changes in

*These authors contributed equally to this work.

photosynthetic antennae that are induced by buildup of a proton gradient across the thylakoid membrane, protonation of PSII subunit S (PSBS), and the conversion of violaxanthin (*V*) to antheraxanthin (*A*) and then zeaxanthin (*Z*) via violaxanthin de-epoxidase (VDE; Yamamoto *et al.*, 1962; Demmig-Adams, 1990; Li *et al.*, 2000). By contrast, low light activates zeaxanthin epoxidase (ZEP), which converts *Z* back to *V*.

Functional diversity for NPQ exists within natural populations (Rungrat *et al.*, 2019), providing opportunities to leverage natural genetic variation to identify additional regulators of known quenching components and/or genes encoding proteins required for additional uncharacterized quenching components. Identifying genes or genomic intervals linked to variation in NPQ requires describing NPQ using a set of multiple distinct numerical traits. The majority of previous attempts to identify natural variants controlling NPQ summarized variation in the trait as a single number corresponding to the maximum level of NPQ observed in the light (Kasajima *et al.*, 2011; Wang *et al.*, 2017) and have focused mainly on a single gene: *PSBS* (Jung & Niyogi, 2009; Kasajima *et al.*, 2011; Wang *et al.*, 2017; Rungrat *et al.*, 2019).

We hypothesized that dissecting the complex NPQ and ΦPSII phenotype into multiple traits describing its kinetics under light and dark conditions in a large, genetically diverse panel would enable us to identify underlying genes. To test our hypothesis, we quantified and parameterized NPQ and ΦPSII kinetics in a replicated panel consisting of world-wide maize accessions. We measured chlorophyll fluorescence from leaf disks collected in 96-well plates and then dark-adapted overnight to minimize the effect of microenvironmental conditions at the time of sampling (i.e. light intensity, temperature, and time of day) and facilitate semi-high-throughput phenotyping. This approach, in combination with genome-wide association studies (GWAS), identified a signal from *PSBS*, as described in other species, as well as numerous additional loci associated with one or more traits of NPQ and ΦPSII kinetics. For six top candidates, we performed validation via gene knockout in Arabidopsis. All analyzed knockouts exhibited changes in NPQ and/or ΦPSII kinetics, suggesting that the mechanisms controlling NPQ and ΦPSII are conserved across $C_4$ and $C_3$ species.

## Materials and Methods

### Field experiments with a maize diversity panel

The field experiments were conducted under dryland conditions at the University of Nebraska-Lincoln's Havelock Research Farm (Lincoln, NE, USA) on silty clay loam soil over two consecutive years, 2020 (40.85°N, 96.62°W) and 2021 (40.86°N, 96.60°W). Each year, a set of > 750 maize (*Zea mays* L.) accessions selected from the Wisconsin Diversity Panel (Hansey *et al.*, 2011; Mazaheri *et al.*, 2019) with a total of 804 unique maize genotypes (a combination of genotypes used in one or both years; Supporting Information Table S1) were grown in a randomized block design (Tables S2, S3). Two blocks of 840 plots for a total of 1680 plots were grown each year. In both years, majority of genotype was present in both blocks. The field included 751 and 782 genotypes in 2020 and 2021, respectively. Each plot consisted of two 2.3-m-long rows of plants from a single genotype. Spacing between rows was 0.76 m, and target spacing between plants within a row was 15 cm. The field was planted on 6 May and 7 May, in 2020 and 2021, respectively. For the details, see Methods S1. In both years, weather data were collected from the Walton 5NW weather station through the High Plains Regional Climate Center website (hprcc.unl.edu; Fig. S1).

### Measuring NPQ and ΦPSII kinetics in field-grown maize plants

NPQ and ΦPSII kinetics were measured in the field-grown maize plants between 31 and 36 d after sowing in 2020 and between 34 and 47 d after sowing in 2021, which corresponded to the pre-flowering stage. The sampling, weather permitting, was performed between 16:00 and 18:30 h. Leaf disks (0.32 $cm^2$) were collected from three plants in the middle of the row of each plot. The disks were cut using a hand-held puncher from the middle portion of the youngest fully expanded leaf and placed immediately, adaxial side down, in a 96-well plate (781611; BrandTech Scientific, Essex, CT, USA). To prevent drying, a moist sponge was placed on top of each leaf disk and the plate was wrapped in aluminum foil followed by an overnight dark incubation at room temperature. The following day, minimum ($F_o$) and maximal ($F_m$) fluorescence in the dark were imaged using a chlorophyll fluorescence imager (FluorCam FC 800-C; Photon Systems Instruments, Drasov, Czech Republic). Subsequently, the plate with the leaf disks was subjected to 10 min of 2000 μmol $m^{-2}$ $s^{-1}$ light (a combination of 1000 μmol $m^{-2}$ $s^{-1}$ of a red-orange light with $\lambda_{max} = 617$ nm and 1000 μmol $m^{-2}$ $s^{-1}$ of a cool white 6500 K light) followed by 10 min of darkness. Saturating flashes of 3200 μmol $m^{-2}$ $s^{-1}$ (provided by a cool white 6500 K light) for a duration of 800 ms were used in the light and dark periods. To capture changes in steady state fluorescence ($F_s$) and maximum fluorescence under illuminated conditions ($F_m'$) over time, saturating flashes were provided at the following intervals (in s): 15, 30, 30, 60, 60, 60, 60, 60, 60, 60, 60, 60, 60, 9, 15, 30, 60, 180, and 300. First, the raw data were processed automatically with fluorescence background exclusion and then NPQ was calculated according to Eqn 1, assuming the Stern–Volmer quenching model (Bilger & Björkman, 1994):

$$\text{NPQ} = F_m/F_m' - 1 \quad \text{Eqn 1}$$

Measured NPQ points largely belonged to two of the fastest component of NPQ named energy-dependent quenching (*qE*) and zeaxanthin-dependent quenching (*qZ*).

Maximum and operating PSII efficiency was estimated from the fluorescence measurements according to Eqns 2 and 3, following Genty *et al.* (1989):

$$\text{Maximum PSII efficiency} = (F_m - F_o)/F_m = F_v/F_m \quad \text{Eqn 2}$$

$$\text{PSII operating efficiency} = (F_m' - F_s)/F_m' = \Phi\text{PSII} \quad \text{Eqn 3}$$

### Parameterization of NPQ and ΦPSII kinetics

To obtain the parameters attributed to the rate, amplitude, and steady state of kinetics, the hyperbola and exponential equations were fit to NPQ kinetics in the light (induction; Eqns 4, 5), or in the darkness (relaxation; Eqns 6, 7; Table S4). Similarly, the recovery of ΦPSII in the darkness was parameterized using the hyperbola (Eqn 8) and exponential equations (Eqn 9). For a complete list of the 25 analyzed parameters and their biological meanings, see Table S4.

$$\mathrm{NPQ} = \frac{\mathrm{time} \times \mathrm{NPQslope}_{\mathrm{lightH}} + \mathrm{NPQasymptote}_{\mathrm{lightH}} - \sqrt{\left(\mathrm{time} \times \mathrm{NPQslope}_{\mathrm{lightH}} + \mathrm{NPQasymptote}_{\mathrm{lightH}}\right)^2 - 4 \times 0.5 \times \mathrm{time} \times \mathrm{NPQslope}_{\mathrm{lightH}} \times \mathrm{NPQasymptote}_{\mathrm{lightH}}}}{(2 \times 0.5)} \quad \text{Eqn 4}$$

$$\mathrm{NPQ} = \mathrm{NPQasymptote}_{\mathrm{lightE}} \times \left(1 - \exp^{\left(-\mathrm{NPQrate\_constant}_{\mathrm{light}} \times \mathrm{time}\right)}\right) \quad \text{Eqn 5}$$

$$\mathrm{NPQ} = \mathrm{NPQsart}_{\mathrm{darkH}} - \frac{\left(\mathrm{time} \times \mathrm{NPQslope}_{\mathrm{darkH}} + \mathrm{NPQamplitude}_{\mathrm{darkH}} - \sqrt{\left(\mathrm{time} \times \mathrm{NPQslope}_{\mathrm{darkH}} + \mathrm{NPQamplitude}_{\mathrm{darkH}}\right)^2 - 4 \times 0.5 \times \mathrm{time} \times \mathrm{NPQslope}_{\mathrm{darkH}} \times \mathrm{NPQamplitude}_{\mathrm{darkH}}}\right)}{(2 \times 0.5)} \quad \text{Eqn 6}$$

$$\mathrm{NPQ} = \mathrm{NPQamplitude}_{\mathrm{darkE}} \times \left(\exp^{\left(-\mathrm{NPQrate\_constant}_{\mathrm{dark}} \times \mathrm{time}\right)}\right) + \mathrm{NPQresidual}_{\mathrm{dark}} \quad \text{Eqn 7}$$

$$\Phi\mathrm{PSII} = \Phi\mathrm{PSIIstart}_{\mathrm{darkH}} + \frac{\left(\mathrm{time} \times \Phi\mathrm{PSIIslope}_{\mathrm{darkH}} + \Phi\mathrm{PSIIamplitude}_{\mathrm{darkH}} - \sqrt{\left(\mathrm{time} \times \Phi\mathrm{PSIIslope}_{\mathrm{darkH}} + \Phi\mathrm{PSIIamplitude}_{\mathrm{darkH}}\right)^2 - 4 \times 0.5 \times \mathrm{time} \times \Phi\mathrm{PSIIslope}_{\mathrm{darkH}} \times \Phi\mathrm{PSIIamplitude}_{\mathrm{darkH}}}\right)}{(2 \times 0.5)} \quad \text{Eqn 8}$$

$$\Phi\mathrm{PSII} = \Phi\mathrm{PSIIamplitude}_{\mathrm{darkE}} \times \left(1 - \exp^{\left(-\Phi\mathrm{PSIIrate\_constant}_{\mathrm{dark}} \times \mathrm{time}\right)}\right) + \Phi\mathrm{PSII}_{\mathrm{startE}} \quad \text{Eqn 9}$$

Fitting the equations to NPQ and ΦPSII data was performed in MATLAB (Matlab R2019b; MathWorks, Natick, MA, USA). Goodness of fit was used to define the discrepancy between measured values and the values expected under the hyperbola and exponential equation fits.

### Phenotype data processing

Best Linear Unbiased Predictors (BLUPs) were calculated for each maize accession in 2020 and 2021 using the formula:

$$Y = \mu + \mathrm{Line} + \mathrm{Plate} + \epsilon$$

where $Y$, $\mu$, Line, Plate, and $\epsilon$ represent phenotype, mean, inbred line effects, plate effects, and the error, respectively. The LME4 R package v.1.1-30 (Bates *et al.*, 2015) was used to obtain BLUPs. Before calculating BLUPs, data from leaf disks with $F_v/F_m$ values lower than 0.65 (2020) or 0.60 (2021) were excluded. The lower $F_v/F_m$ value was chosen for quality control of data in 2021 due to the drier and hotter growing environment that year (Fig. S1). Furthermore, measurements with poor fit (below the 1st percentile of the goodness of fit in 2020 and below the 1.5th percentile of the goodness of fit in 2021) were also excluded. Additionally, outliers with extremely high slopes of the NPQ and/or ΦPSII curves were discarded. Finally, 26 disks in 2020 and two in 2021 were removed due to the low fluorescence signal. In total, these criteria removed 698 of 4506 leaf disks in 2020 and 1565 of 4665 leaf disks in 2021.

### Genome-wide association analysis

Genetic marker data were taken from the set of 899 784 SNPs published for the Wisconsin Diversity Panel (Mazaheri *et al.*, 2019). After filtering to remove SNPs with a minor allele frequency below 5% among the subset of the Wisconsin Diversity Panel employed in this study, a total of 428 487 SNPs were retained for downstream analyses. The genetic marker data and BLUP values described above were employed for the GWAS via the Fixed and random model Circulating Probability Unification (FarmCPU) algorithm as implemented in RMVP v.1.0.6 (Liu *et al.*, 2016; Yin *et al.*, 2021). Analysis for each trait included the first five principal components calculated from marker data as covariates. For each trait, a resampling analysis was conducted to assess the stability of significant associations (Valdar *et al.*, 2009). Separate genome-wide association tests were performed for 100 random samples, each including 80% of the total number of

genotyped and phenotyped maize associations. A *P*-value of *c.* $10^{-6.93}$, corresponding to a Bonferroni corrected $\alpha = 0.05$ after correcting for multiple testing on 428 487 markers, was used to determine whether a given SNP was considered to be statistically significantly linked to phenotypic variation in a given random sample. For each genetic marker, the proportion of these 100 analyses where the marker exhibited a statistically significant association with the trait of interest (resampling model inclusion probability (RMIP)) was determined.

### eQTL and transcriptome-wide association analyses

Previously published expression data for the Wisconsin Diversity Panel (Gage *et al.*, 2019) contain two clusters samples with substantially different patterns of expression corresponding to lines sequenced as part of Hirsch *et al.* (2014) and those sequenced as part of Mazaheri *et al.* (2019). eQTL analysis was conducted using the unified mixed-model as implemented in rMVP v.1.0.6 (Yu *et al.*, 2006; Yin *et al.*, 2021) with five principal components calculated as from the genotype matrix, kinship, and a batch effect corresponding to which study the RNA-Seq data was originally generated in either Hirsch *et al.* (2014) or Gage *et al.* (2019) were incorporated as covariates in the model. The FPKM (fragments per kilobase of exon per million reads) values for each of the candidate genes evaluated were used as phenotypes and the same set of 428 487 SNPs described in the previous section were used as the marker set. For transcriptome-wide association study (TWAS), the same expression data matrix was filtered first to include only those lines sequenced as part of the Hirsch *et al.* (2014) study which overlapped with the line phenotype in our field experiment (368 total) and to remove genes with expression of 0 in > 50% lines, leaving a set of 27 372 genes. A linear model was fit to the relationship between the expression of each gene to the observed values for each phenotype across the set of maize genotypes for which expression data were available and NPQ-related traits had been collected. For each linear model, the first five principal components calculated from the genetic marker dataset were fit as covariates. A *P*-value threshold of *c.* $10^{-5.74}$, corresponding to a Bonferroni corrected $\alpha = 0.05$ after correcting for multiple testing on 27 372 genes, was used to determine whether a given gene was considered to be statistically significantly linked to phenotypic variation. The custom R code used to implement the TWAS model described above is provided in the github repository associated with this study. Nonsynonymous SNPs and InDels present within candidate genes were identified using the resequencing dataset and variant calls described in Grzybowski *et al.* (2023) and SnpEff v.5.1 (Cingolani *et al.*, 2012). Calculations of linkage disequilibrium were performed using Plink v.1.90 (Purcell *et al.*, 2007).

### Arabidopsis mutants to verify the candidate genes

Maize genes were mapped to their Arabidopsis (*Arabidopsis thaliana*) orthologs using the 'xref' annotation data provided on Phytozome (https://phytozome-next.jgi.doe.gov/) as part of a set of genome files for B73 RefGen_v.4. Six candidate genes were validated in the following Arabidopsis T-DNA insertional mutants: *acht3* (SALK_062853 for *ATYPICAL CYS HIS RICH THIOREDOXIN 3*; At2g33270), *irm1* (SALK_106042 for *INCREASED RESISTANCE TO MYZUS PERSICAE 1*; At5g65040), *oep37* (SALK_147406 for *CHLOROPLAST OUTER ENVELOPE PROTEIN 37*; At2g43950), *pmi1* (SALK_141795 for *PLASTID MOVEMENT IMPAIRED 1*; At1g42550), *psi3* (SALK_086423 (*psi3-1*) and SALK_114872 (*psi3-2*) for *PHYTOSULFOKINE SIMULATOR 3*; At5g08660), and *trx-y1* (SALK_035609 for *THIOREDOXIN Y1*; At1g76760; Alonso *et al.*, 2003). The seeds of all T-DNA insertional mutants and their corresponding WT (CS6000) were obtained from the Arabidopsis Biological Resource Center (ABRC) at Ohio State University. The lines were selfed at least once or until homozygous progeny for the T-DNA insertion were confirmed by PCR. The RT-PCR was used to confirm that the T-DNA insertion abolished expression of the mature transcript. For details, see Methods S2, Fig. S2 and Table S5.

### Arabidopsis growth conditions

Seeds of Arabidopsis (*Arabidopsis thaliana* L.) mutants and their corresponding WT were stratified at 4°C for 4 d. Stratified seeds were placed in 10 × 10 cm pots (12140400; Hummert International, Earth City, MO, USA) filled with potting mix (1220338; BM2 Germination and Propagation Mix; Berger, Saint-Modeste, Canada), which were placed in a tray (6569630; Hummert International) filled with *c.* 2 cm of water at the bottom and covered with a clear plastic dome (65696400; Hummert International) until germination. The trays were placed in a controlled-environment reach-in growth chamber (AR-66L2; Percival, Perry, IA, USA) set to a 10 h : 14 h, day : night, 21°C : 18°C photoperiod, 60% relative humidity with the light controlled at 150–200 μmol $m^{-2}$ $s^{-1}$. Plants were repositioned randomly twice a week and watered with 150 ppm liquid fertilizer (Peter's 20–10–20 general purpose fertilizer, 25#, Peters Inc., Allentown, PA, USA). The growth under the 700 μmol $mol^{-1}$ of $CO_2$ was conducted in a controlled-environment walk-in growth chamber (BDW40; Conviron, Pembina, ND, USA). The $CO_2$ enrichment started when seedlings were 7-d-old. Other details of plant growth were as stated above.

### NPQ and ΦPSII kinetics in Arabidopsis mutants

The NPQ and ΦPSII kinetics were measured and parametrized as described above with a few modifications. The fluorescence images were taken of whole 4-wk-old plants after 20 min of dark adaptation. Saturated pulses of 2400 μmol $m^{-2}$ $s^{-1}$ and actinic light of 1000 μmol $m^{-2}$ $s^{-1}$ (a combination of 500 μmol $m^{-2}$ $s^{-1}$ of a red-orange light with $\lambda_{max} = 617$ nm and 500 μmol $m^{-2}$ $s^{-1}$ of a cool white 6500 K light) were used. Mutants were grown in three batches each with WT plants. For data analysis, from each plant, an area of 270–280 pixels was chosen manually from the portion of three of the youngest, fully expanded leaves facing the illumination panel.

### Photosynthetic gas exchange measurements in Arabidopsis mutants

The light dose–response curves of leaf net $CO_2$ assimilation ($A_n$) and linear electron transport ($J$) were determined on 4-wk-old plants grown under ambient and elevated $CO_2$ (700 μmol $mol^{-1}$) conditions by measuring gas exchange and pulse amplitude-modulated chlorophyll fluorescence at a broad range of light intensities using an open gas exchange system LI-6800 (Li-Cor Inc., Lincoln, NE, USA) equipped with a 2-$cm^2$ leaf cuvette chamber and an integrated modulated fluorometer. Block temperature, [$CO_2$] inside the cuvette, and water vapor pressure deficit were controlled at 23°C, 400, or 700 μmol $mol^{-1}$ and 1.1 kPa, respectively. A young fully expanded leaf was closed in the leaf cuvette and dark-adapted for 20 min, after which $F_o$ and $F_m$ were recorded to calculate $F_v/F_m$ (Eqn 2). Next, using 90% red and 10% blue LEDs the light intensity was slowly increased from 0 to 50, 80, 110, 140, 170, 200, 300, 400, 500, 700, 800, and 1000 μmol $m^{-2}$ $s^{-1}$ of the incident photon flux density (PFD; Fig. S3a). When a steady state was reached, $A_n$, stomatal conductance ($g_s$), $F_s$, and $F_m'$ parameters were recorded. A multiphase flash routine was used to record all fluorescence parameters (Loriaux *et al.*, 2013). From the fluorescence data, NPQ and ΦPSII were calculated according to Eqns 1 and 3, respectively. In addition to steady state, a dynamic light response curve was reconstructed from the timed series of changes in light intensity. After leaves reached the steady state of gas exchange parameters at 1000 μmol $m^{-2}$ $s^{-1}$ PFD, the light intensity was changed from 1000 to 800, 700, 500, 400, 300, 200, 170, 140, 110, 80, and 50 μmol $m^{-2}$ $s^{-1}$ PFD, where each step lasted 4 min and was preceded by 4 min of 1000 μmol $m^{-2}$ $s^{-1}$ PFD (Fig. S3b). At each light intensity, gas exchange and fluorescence parameters were recorded after 80, 160, and 240 s. The values of these three measurements were averaged to reconstruct light response curves under fluctuating light.

Both types of light response curves were analyzed in a similar way. The rate of linear electron transport ($J$) was estimated according to Eqn 10:

$$J = 0.843 \times \Phi PSII \times PFD \times 0.5 \qquad \text{Eqn 10}$$

where partitioning of absorbed irradiance between the two photosystems is assumed to be 0.5 and 0.843 is the leaf absorption weighted to 90% red and 10% blue light.

The quantum efficiency of linear electron transport and the quantum efficiency of leaf net $CO_2$ assimilation were derived from the initial slope of the light response of $J$ and $A_n$, respectively. $A_{sat}$ and $J_{max}$ were asymptotes of the nonrectangular hyperbola fit to the light responses of $A_n$ and $J$, respectively (Long & Bernacchi, 2003).

To analyze the $CO_2$ response of $A_n$, leaves were clamped in the cuvette with block temperature controlled at 23°C and light intensity set at 1200 μmol $m^{-2}$ $s^{-1}$ PFD. $CO_2$ concentration in the cuvette was set to 13 subsequent values 400, 300, 200, 100, 75, 400, 400, 500, 600, 800, 1000, 1200, and 1500 μmol $mol^{-1}$, and gas exchange parameters were logged when steady state was reached. A model for leaf photosynthesis (Farquhar *et al.*, 1980) with temperature corrections (Sharkey *et al.*, 2007) was fitted to the response of $A_n$ to intercellular $CO_2$ concentration ($C_i$) to estimate the maximal carboxylation rate ($V_{cmax}$), linear electron transport rate ($J$), and triose phosphate utilization rate (TPU).

### Statistical analyses

Statistical analyses of NPQ and ΦPSII kinetics and gas exchange measurements in Arabidopsis mutants were performed in SAS (v.9.4, SAS Institute Inc., Cary, NC, USA). Data were tested with the Brown–Forsythe test for homogeneity of variance and the Shapiro–Wilk test for normality. If the null hypothesis was discarded by either test, data were transformed or the Wilcoxon nonparametric test was applied. Significant effects by one-way ANOVA ($\alpha = 0.05$) were followed by testing mutant means against the WT control ($\alpha = 0.05$) using Dunnett's test with a multiple comparison correction.

## Results

### Diversity of NPQ and ΦPSII traits in field-grown maize

In 2020, of 4506 collected leaf disks, data for 3808 samples passed quality control (see the Materials and Methods section for more details) and were used for downstream analyses. We observed substantial differences across maize genotypes for NPQ and ΦPSII at individual time points and in the shapes of NPQ and ΦPSII curves (Figs 1a,b, S4). An example of the range of NPQ kinetics observed across the diversity panel as a whole is presented in Fig. 1(a,b). Inbred line B73 exhibited a slow rate of NPQ induction, a moderate maximum value, and rapid relaxation as well as the lowest value of NPQ after 10 min in the dark. Inbred line LH132 also exhibited a slow rate of NPQ induction, comparable to that of B73; however, LH132 reached a much higher maximum NPQ value over the 10-min high-light period. By contrast, lines PHGV6 and PHP76 exhibited rapid NPQ induction but PHGV6 reached a much higher NPQ value than PJHP76, combined with a substantially faster rate of relaxation and higher NPQ residual in the dark period. We calculated broad-sense heritability for each of the 25 analyzed traits ($H^2$; Table S4) as well as the correlation between NPQ related traits and a set of manually measured traits of interest measured from the same population of maize lines (Mural *et al.*, 2022; Fig. S5).

### Identification of candidate genes involved in NPQ and ΦPSII in maize

We conducted a GWAS using the Fixed and random model Circulating Probability Unification (FarmCPU) algorithm with resampling to identify genomic intervals associated with variation in NPQ and/or ΦPSII among the maize genotypes in the 2020 field experiment. Using a previously published dataset of 428 487 SNPs (see the Materials and Methods section), a total of 18 unique single-nucleotide polymorphisms (SNPs), each associated with one or more traits, were identified above the confidence

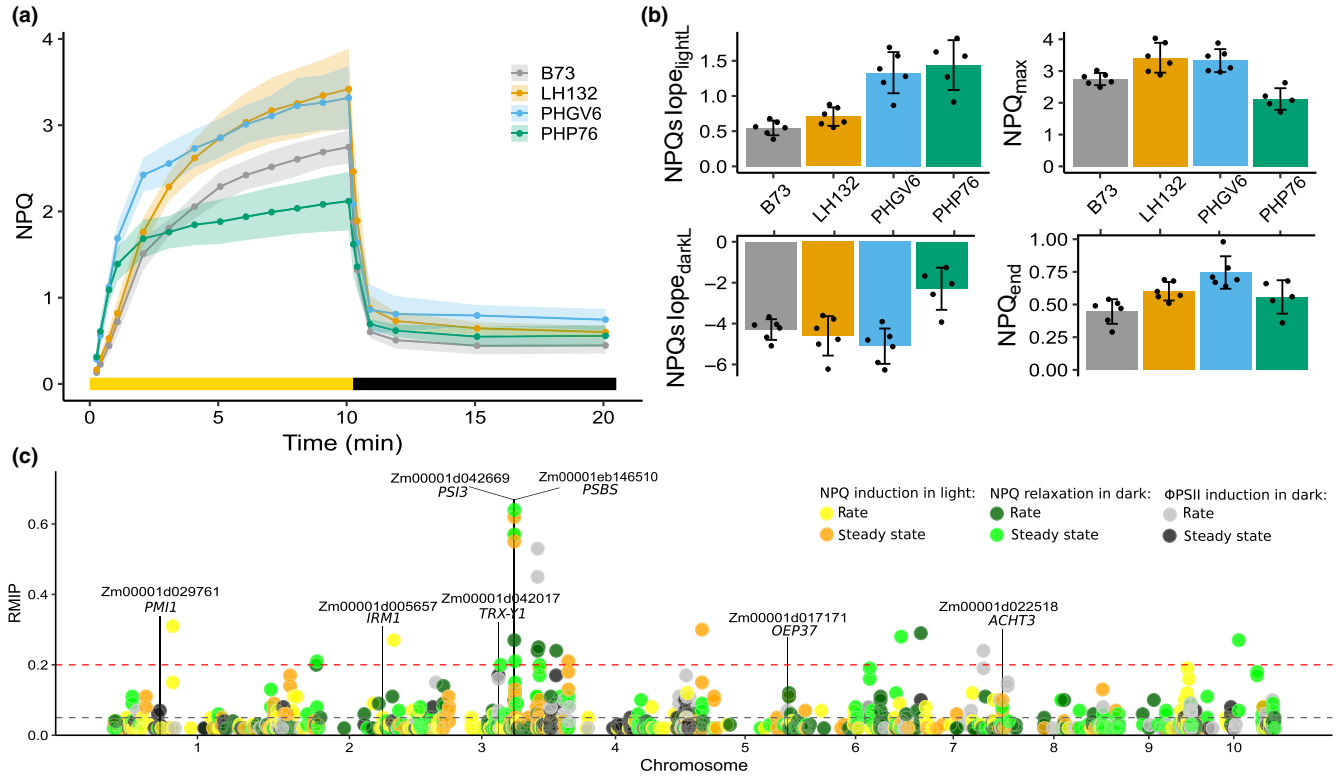


**Fig. 1** Nonphotochemical quenching (NPQ) kinetics observed in selected genotypes from the maize diversity panel and genetic loci controlling variation in NPQ and photosystem II (PSII) operating efficiency (ΦPSII). (a) Changes in NPQ during induction in the light (indicated by the yellow horizontal bar) and during relaxation in darkness (indicated by the black horizontal bar) in four maize genotypes representing the range of curves observed among a maize diversity panel: B73, the maize reference genotype; LH132, an expired patented line developed by Bayer (previously Monsanto); and PHGV6 and PHP76, two expired patented lines developed by Corteva (previously Pioneer Hi-Bred). The shaded area around the curves presents ±SD of the mean. (b) Differences in four NPQ traits observed between genotypes and among biological replicates. $NPQslope_{lightL}$, initial slope of linear function fit to zero and the first two points for NPQ induction in the light; $NPQslope_{darkL}$, initial slope of linear function fit to the last point in the light and the first two points in darkness for NPQ relaxation; $NPQ_{max}$, the highest value of NPQ during induction; and $NPQ_{end}$, NPQ in the last point of relaxation. Traits correspond to NPQ curves shown in (a). Data are means ± SD and points represent single measurements. (c) Results from a set of resampling-based GWAS conducted for 25 individual traits calculated from the observed NPQ and ΦPSII curves of 746 maize genotypes grown in a replicated field trial in Lincoln, NE in 2020. The *x*-axis indicates the position of a given marker on the maize genome pseudomolecules (B73_RefGen_V4). The *y*-axis indicates the resampling model inclusion probability (RMIP). Only markers with a RMIP ≥ 0.02 are shown. The maximum potential RMIP was 1.0. The *y*-axis is truncated at 0.75 to improve readability. RMIP values ≥ 0.05 were considered sufficiently suggestive to justify characterization of nearby candidate genes (dashed gray line). RMIP values ≥ 0.2 were considered strong evidence of an association between the genomic interval and the trait(s) of interest (dashed red line). The positions of *PSBS*, known to influence NPQ, and six candidate genes investigated in this study are indicated with solid black vertical lines and are described in Supporting Information Table S8. Data used to produce this figure are given in Dataset S1.

threshold of association (resampling model inclusion probability (RMIP) ≥ 0.2) and an additional 185 unique SNPs at a suggestive association threshold (RMIP ≥ 0.05; Table S6). We detected 221 genes located within 10 kb of the 203 SNPs associated with variation in NPQ and/or ΦPSII in this maize panel (Table S7). The single most significant signal originated from a SNP located in Zm00001d042669, a maize ortholog of Arabidopsis *PSI3*, referred to as *PSI3* below, at position 176 152 936 on maize chromosome 3, which was 1.2 Mb upstream from *PSBS* (Zm00001d042697; Fig. 2a). The SNP located in *PSI3* was significantly associated with eight out of the 25 analyzed traits: three describing the steady state of NPQ induction, two describing the rate of NPQ relaxation, two describing the range of NPQ relaxation, and one trait contributing to the range of NPQ relaxation (Table S8). *PSBS* is associated with variation in the maximum NPQ in different species (e.g. Wang *et al.*, 2017; Rungrat *et al.*, 2019). We also identified *PSBS* as being associated with multiple traits describing the steady state of NPQ induction and the rate of NPQ relaxation (Table S8) and *PSBS* was the sole significant signal, after correcting for multiple testing, recovered in a TWAS analysis use the NPQ-related phenotypes measured here and a previously published set of gene expression data from maize v1 seedlings (Fig. S6).

In addition to *PSI3*, five other genes were chosen for validation based on their high association with the analyzed traits (Fig. 1c; Table S8), *Atypical Cys His Rich Thioredoxin 3* (*ACHT3*) and *Thioredoxin Y1* (*TRX-Y1*) both encode thioredoxins but previous mutant work had not linked either gene to photosynthetic or NPQ-related traits (Dangoor *et al.*, 2009; Vanacker *et al.*, 2018; Chibani *et al.*, 2021). A very similar set of traits to the ones significantly associated with the SNP located within *PSBS* were also significantly associated with a SNP located within *ACHT3*. We detected a significant association between four traits related to the kinetics of NPQ and ΦPSII in the darkness and a SNP

New Phytologist

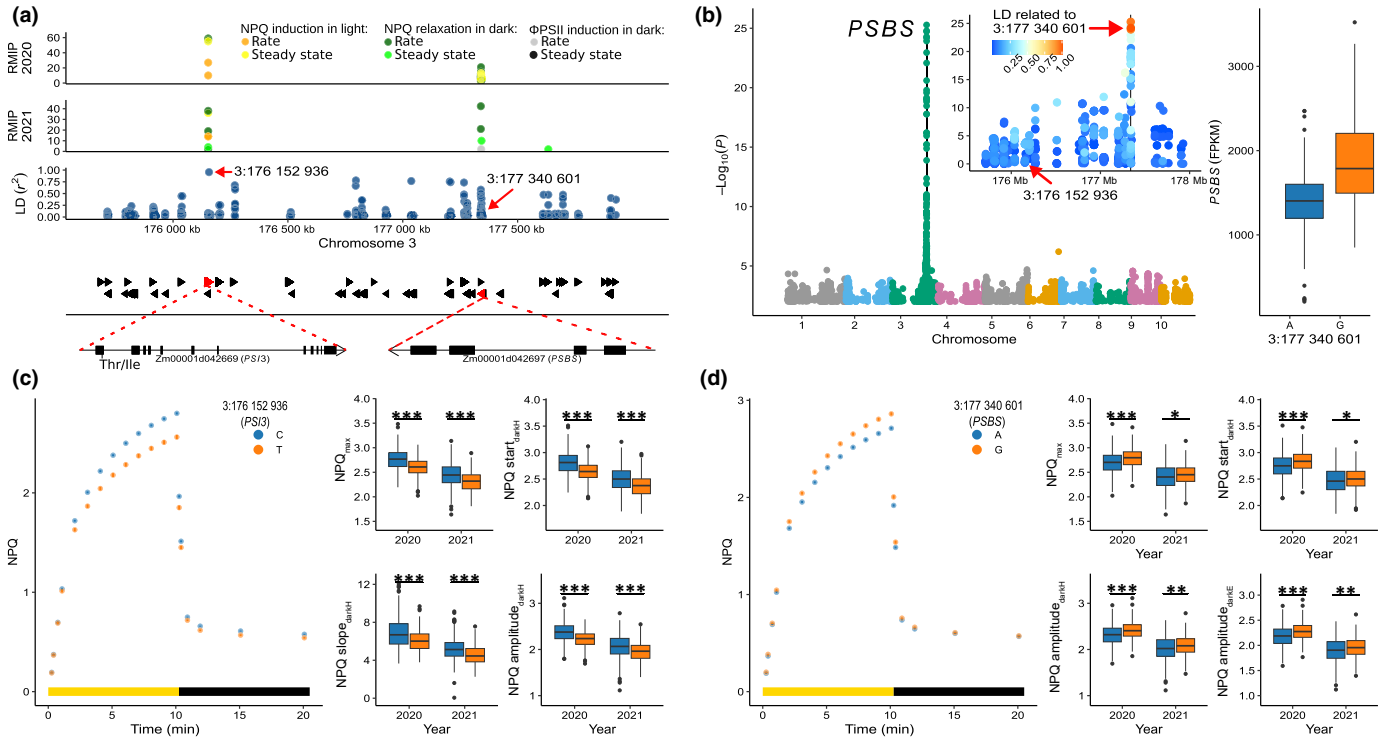


**Fig. 2** Characterization of the known nonphotochemical quenching (NPQ) gene *PSBS* and the candidate NPQ gene *PSI3* in maize. (a) A zoomed in the *c*. 2.3 Mb window containing Zm00001d042669 (*PHYTOSULFOKINE SIMULATOR 3*; *PSI3*) and Zm00001d042697 (*PHOTOSYSTEM II SUBUNIT S*; *PSBS*). Top panel shows a zoomed view of the results of genome-wide association study (GWAS) conducted using NPQ phenotypes measured in the field in 2020 from Fig. 1(c). The second panel from the top displays the results of a separate GWAS conducted using phenotypes scored in 2021 (a second environment). The third panel shows the linkage disequilibrium (LD) between SNPs in this region and the peak SNP located within *PSI3* 3:176152936, marked with red arrow. The second SNP marked in this panel (3:177340601) is the peak SNP identified within *PSBS* which is not in LD with the *PSI3* SNP. The third panel from the top also displays the distribution of annotated genes within this 2.3-Mb window with the two genes of interest marked in red. The final panel displays the structural annotations of each gene with nonsynonymous mutations identified from resequencing data in > 0.5 LD with GWAS hits marked in red. (b) Results of an expression GWAS conducted for *PSBS* expression, using a mixed linear model, which identified a *cis*-eQTL colocalized with *PSBS*. The position of *PSBS* is indicated by a vertical black line. Inset panel displays a zoomed in the expression GWAS results in the *PSBS* region with the two SNPs identified from NPQ GWAS indicated by red arrows. Distribution of observed expression levels for individuals carrying different alleles of the SNP within *PSBS* identified from GWAS for NPQ traits are shown in the right-hand portion of this panel. (c) (Left) Differences in pattern of observed NPQ responses for individuals carrying either the C (reference) or T (alternative) alleles of SNP 3:176152936 (located within *PSI3*). Error bars, indicating SE, are plotted for each point but frequently are smaller than the symbol size. (Right) Distributions of phenotypic values calculated from NPQ curves for individuals carrying either the C (reference) or T (alternative) alleles in both the 2020 field season and a second replicated field study conducted in 2021. (d) Differences in pattern of observed NPQ responses for individuals carrying either the C (reference) or T (alternative) alleles of SNP 3:177340601 (located within *PSBS*). Data are displayed as described in panel (c). Unpaired two-tailed *t*-test: *, $P < 0.05$; **, $P < 0.01$; ***, $P < 0.001$. In the boxplot graphs (panels b–d), the points, horizontal lines, and whiskers represent outliers, median, and the line drown from the top of the box to the largest and from the bottom of the box to the smallest values within 1.5 interquartile range, respectively. Data used to produce this figure are given in Supporting Information Datasets S1 and S2.

located within *TRX-Y1*. *Plastid Movement Impaired 1* (*PMI1*) encodes a plant-specific protein involved in chloroplast relocatization in response to high light (DeBlasio *et al.*, 2005; Dwyer & Hangarter, 2022). *Chloroplast Outer Envelope Protein 37* (*OEP37*) encodes a cation-selective, high-conductance channel in the outer envelope of plastids (Ferro *et al.*, 2002; Goetze *et al.*, 2006). SNPs located within *OEP37* and *PMI1* were significantly associated with traits describing the rate and range of ΦPSII induction in dark conditions. *Increased Resistance to Myzus Persicae 1* (*IRM1*) appears to play a role in insect resistance but was previously linked to variation in $F_v/F_m$ in an Arabidopsis GWAS study (Oakley *et al.*, 2018). In all six genes selected for mutant validation in Arabidopsis, the SNP identified by GWAS was located within the gene itself (Figs 2a, S7). In three cases (*IRM1*, *PMI1*, and *OEP37*), no other genes were within 10 kb of the SNP tagged by GWAS (Fig. S7). While exceptions exist, functional variants in the genome typically influence phenotype either by changing the sequence of a protein in a way that alters function or by changes in the abundance of a given protein as a result of changes in transcriptional regulation. Whole-genome resequencing data for a large set of maize genotypes recently became available (Grzybowski *et al.*, 2023). While numerous segregating missense or nonsense variants were observed in *PSBS*, *PSI3*, and the other candidate genes, in only three cases was a nonsynonymous SNP in high LD (> 0.5) with the SNP identified via GWAS analysis (Table S9; Figs 2a, S7). The greatest LD between a GWAS hit and a nonsynonymous sequence change was observed in *PSI3*, which contains a threonine to isoleucine substitution in LD of 0.93 with the SNP tagged by GWAS within that gene (Fig. 2a). Expression quantitative trait locus

(eQTL) analysis identified eQTL for *PSBS* (Fig. 2b) and four of the six candidate genes (*IRM1*, *TRX1-Y1*, *PMI1*, and *OEP37*), that colocalized the annotated positions of these genes in the genome (Fig. S8). In all six cases, at least one plausible type of functional variation was observed.

## Consistent effects of SNPs on NPQ and ΦPSII traits across two growing seasons

Many significant genetic associations observed in single-year studies fail to replicate in subsequent studies due to genotype-by-environment interactions. Therefore, we performed a second round of phenotyping of NPQ and ΦPSII traits in 2021 using the same maize panel grown in a different field in Lincoln, NE (40.86N, 96.60W) to evaluate the stability of the genetic signals identified in 2020. In Lincoln, 2021 was hotter and much drier than in 2020, exposing the maize plants to increased environmental stress (Fig. S1). We collected 4665 leaf disks in 2021 and 3100 samples passed quality control and were used for downstream analyses. We grew and measured most of the investigated genotypes (712 out of 751) in both growing seasons. Pearson's correlations between individual NPQ and ΦPSII traits measured in the same genotypes in 2020 and 2021 were modest, ranging from $r = 0.17$ ($\Phi PSII_{startH}$) to $r = 0.52$ (NPQrate_constant$_{dark}$; Fig. S9). Nevertheless, *PSBS*, *PSI3* (Figs 2c,d, S10), and the four of the five other genes selected for downstream validation based on the GWAS conducted using 2020 data had consistent and significant ($P \leq 0.05$) effects across both years on all NPQ and ΦPSII traits significantly associated with them (RMIP $\geq 5$; Figs S11–S14). The only exception was the SNP within *OEP37* associated with variation in ΦPSIIrate_constant$_{dark}$ in 2020, as it failed to show an association in 2021 (Fig. S15). An independent genome-wide association study conducted using only 2021 data identified consistent signals from *PSBS* and *PSI3* as well as an additional strong signal associated with Zm00001d053675 (*Lipoxygenase 10*; *LOX10*), a gene associated with only a moderate GWAS hit in 2020 (Fig. S16; Tables S10, S11).

## Validation of candidate genes using Arabidopsis T-DNA insertional mutants

Next, we identified the Arabidopsis orthologs for the six candidate maize genes and investigated the following T-DNA insertional mutants: *acht3*, *irm1*, *oep37*, *pmi1*, *psi3-1*, *psi3-2*, and *trx-y1*. We used PCR to confirm the T-DNA insertion and homozygosity in the mutants and reverse transcription PCR (RT-PCR) to verify the lack of full-length transcripts in plants carrying the T-DNA insertions (Figs S17, S18).

To test the effect of these gene knockouts on NPQ, we investigated NPQ kinetics in fully developed leaves of the mutants in light and dark conditions. Each mutant line exhibited a slower rate of NPQ induction and lower steady-state NPQ in the light relative to the wild-type (WT) control (Fig. 3a–f). Similarly, in the darkness, the rate of NPQ relaxation was slower and the range of the NPQ response was smaller in mutant lines than in WT plants. The individual mutants exhibited significant differences ($P \leq 0.04$) from the WT in at least seven out of 14 analyzed NPQ traits (Figs 3g–l, S19a–h). One exception was *psi3-2*, which differed significantly from the WT only in $NPQ_{max}$ ($P = 0.017$). By contrast, *psi3-1* had significantly lower values for eight out of 14 NPQ parameters ($P \leq 0.002$). In the mutants, the rate of NPQ relaxation showed, on average, the highest decrease (Figs 3i, S19e,f). For instance, $NPQslope_{darkH}$, on average, decreased by 20% (from −29% in *trx-y1* ($P = 0.004$) to 9% in *acht3* ($P = 0.13$)) relative to the WT. NPQ in the last time point measured ($NPQ_{end}$) was the only NPQ parameter for which some lines showed an increase and others a decrease, with *acht3* (28%; $P = 0.0006$) and *psi3-1* (−20%; $P = 0.002$) exhibiting significant changes compared with the WT.

In the mutants, the kinetics of ΦPSII recovery in the dark was much less affected than NPQ (Figs S19j–m, S20); nevertheless, three lines showed significant differences compared with the WT. The *pmi1* mutant had a 5% higher range of ΦPSII induction ($\Phi PSII_{end}/\Phi PSII_{start}$, $P = 0.004$) than the WT (Fig. S20k). The *psi3-1* mutant showed a significant alteration in three ΦPSII traits, with the rate of ΦPSII recovery ($\Phi PSIIslope_{darkH}$, −26%) and $\Phi PSII_{end}/NPQ_{end}$ (−28%) being most affected ($P \leq 0.009$; Fig. S20h,k,l). Out of the four ΦPSII kinetics traits that were significantly affected in *acht3*, the ratio between ΦPSII and NPQ at the end of the dark period ($\Phi PSII_{end}/NPQ_{end}$) had the most significant reduction by 23% ($P = 0.0006$; Figs S19j, S20g,j,l).

For four (*PSI3*, *TRX-Y1*, *ACHT3*, and *IRM1*) of the six candidate genes, traits describing the same attributes of NPQ and/or ΦPSII kinetics were significantly affected in maize and Arabidopsis. For instance, the steady state of NPQ in the light and the amplitude of NPQ relaxation in the dark were significantly affected by the SNP in *PSI3* in maize and by the T-DNA insertion in the Arabidopsis *psi3-1* mutant (Figs 2c, 3h,j,k, S10, S19c,d,g).

## Effect of *PSI3* on photosynthetic efficiency in Arabidopsis

*PSI3* exhibited one of the strongest associations with natural variation of NPQ in maize. To assess whether the *AtPSI3* knockout also affects photosynthesis, we performed a series of gas exchange measurements on the Arabidopsis *psi3* mutants (Fig. 4). Relative to the WT, the *psi3-1* mutant differed significantly in the response of NPQ to gradual changes in light, and the direction of these differences strongly depended on light intensities (Fig. 4a). For instance, at 200 μmol $m^{-2}$ $s^{-1}$, *psi3-1* had a 62% higher NPQ ($P = 0.019$), and at 800 μmol $m^{-2}$ $s^{-1}$, *psi3-1* had a 10% lower NPQ ($P = 0.04$) than the WT (Fig. 4c,d). Furthermore, the electron transport rate ($J$) was strongly impaired in *psi3-1* at a broad range of light intensities (from −4% to −24% at incident photon flux density (PFD) $\geq 110$ μmol $m^{-2}$ $s^{-1}$; $P \leq 0.038$; Fig. 4a,b). However, the quantum efficiency of leaf net $CO_2$ assimilation and quantum efficiency of linear electron transport were not significantly different ($P \geq 0.3$) from those of the WT (Fig. 4b). The decrease in $J$ and ΦPSII was associated with a significant reduction in stomatal conductance (−35% to −52% at a PFD $\geq 0$ μmol $m^{-2}$ $s^{-1}$; $P \leq 0.005$) and a significant decrease in

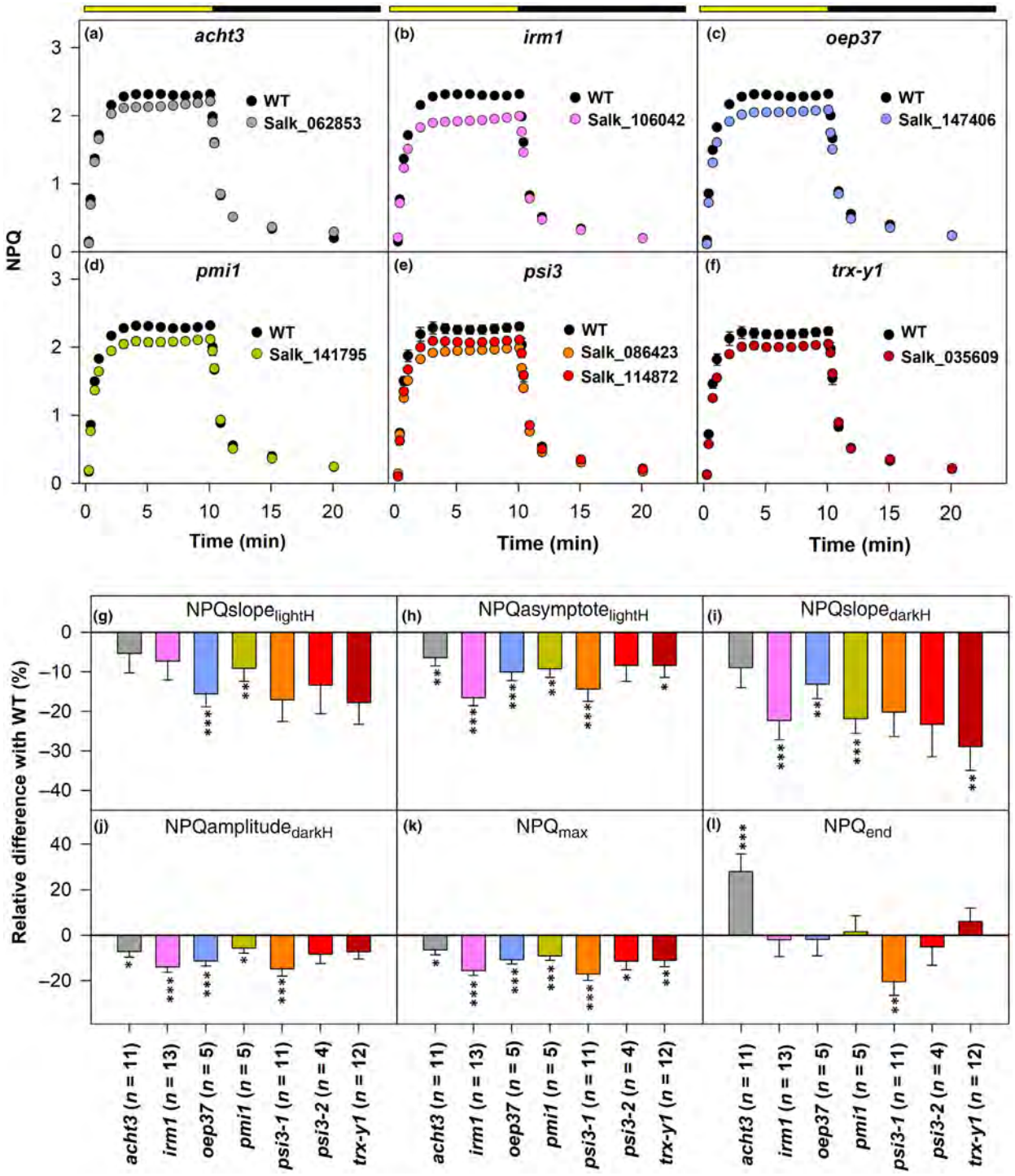


**Fig. 3** Validation of six candidate genes in Arabidopsis T-DNA insertional mutants based on six NPQ traits. Nonphotochemical quenching (NPQ) was measured in the mutants (a) *acht3* (*ATYPICAL CYS HIS RICH THIOREDOXIN 3*; SALK_062853), (b) *irm1* (*INCREASED RESISTANCE TO MYZUS PERSICAE 1*; SALK_106042), (c) *oep37* (*CHLOROPLAST OUTER ENVELOPE PROTEIN 37*; SALK_147406), (d) *pmi1* (*PLASTID MOVEMENT IMPAIRED1*; SALK_141795), (e) *psi3* (*PHYTOSULFOKINE SIMULATOR 3*; SALK_086423 (*psi3-1*) and SALK_114872 (*psi3-2*)), and (f) *trx-y1* (*THIOREDOXIN Y1*; SALK_035609), as well as the corresponding wild-type (WT; CS60000). In panels (a–f), NPQ induction during a 10-min exposure to light (1000 µmol $m^{-2}$ $s^{-1}$; indicated by the yellow horizontal bar) is followed by NPQ relaxation during 10 min of darkness (indicated by the black horizontal bar); NPQ traits derived from the curves shown in panels (a–f): (g) initial slope ($NPQslope_{lightH}$) and (h) asymptote ($NPQasymptote_{lightH}$) of hyperbola fit to NPQ induction; (i) initial slope ($NPQslope_{darkH}$) and (j) amplitude ($NPQamplitude_{darkH}$) of hyperbola fit to NPQ relaxation; (k) the highest value of NPQ during induction ($NPQ_{max}$) and (l) NPQ in the last point in dark ($NPQ_{end}$). Panels (g–l) show data normalized to corresponding WT plants grown in the same batch. Mutants *acht3* and *irm1* were grown with $n = 12$ WT plants, *oep37*, and *pmi1* were grown with $n = 6$ WT plants, and *psi3* and *trx-y1* were grown with $n = 8$ WT plants. Data are means ± SE ($n$ from 4 to 13 biological replicates), and asterisks indicate significant differences between WT and mutants based on Dunnett's two-way test: *, $P \leq 0.05$; **, $P \leq 0.01$; ***, $P \leq 0.001$. Data used to produce this figure are given in Supporting Information Dataset S3.

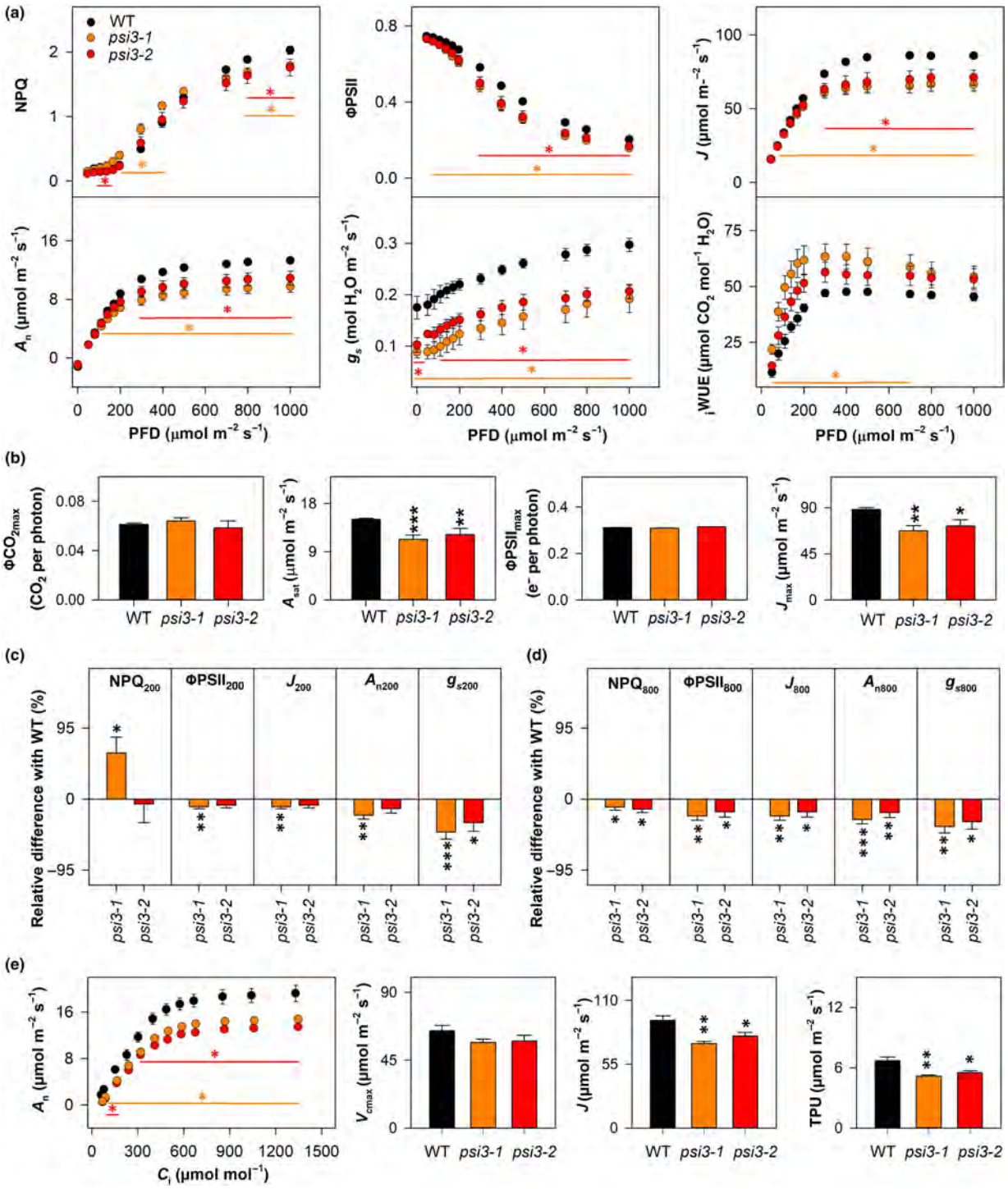


**Fig. 4** Response of photosynthesis-related parameters to gradual changes in light and intercellular $CO_2$ concentration in Arabidopsis *psi3-1* and *psi3-2* T-DNA insertional mutants and the corresponding wild-type (WT). (a) Nonphotochemical quenching (NPQ), photosystem II operating efficiency (ΦPSII), linear electron transport rate (*J*), net $CO_2$ fixation rate ($A_n$), stomatal conductance ($g_s$), and intrinsic water-use efficiency ($_i$WUE) as a function of incident photon flux density (PFD). (b) Quantum efficiency of leaf net $CO_2$ assimilation ($\Phi CO_{2max}$), light-saturated rate of net assimilation rate ($A_{sat}$), quantum efficiency of linear electron transport ($\Phi PSII_{max}$), and maximal linear electron transport rate ($J_{max}$). NPQ, ΦPSII, *J*, $A_n$, and $g_s$ were measured at a light intensity of (c) 200 and (d) 800 μmol $m^{-2}$ $s^{-1}$. (e) $A_n$ as a function of intercellular $CO_2$ concentration ($C_i$) and maximum ribulose bisphosphate carboxylation capacity ($V_{cmax}$); rate of linear electron transport (*J*) and rate of triose phosphate utilization (TPU). Data are means ± SE (*psi3-1*, *n* from 6 (panel e) to 7 (panels a–d); *psi3-2*, *n* from 4 (panels a–d) to 6 (panel e) and wild-type (WT), *n* from 7 (panel e) to 8 (panels a–d) biological replicates). In panel (c), data were normalized to measurements of the corresponding WT. In panels (a, e), asterisks/lines show significant differences from the WT (orange for *psi3-1* and red for *psi3-2*; Dunnett's two-way test: $P \leq 0.05$). In panels (b–e), black asterisks indicate significant differences between the WT and mutants based on Dunnett's two-way test: *, $P \leq 0.05$; **, $P \leq 0.01$; ***, $P \leq 0.001$. Data used to produce this figure are given in Supporting Information Datasets S4 and S6.

$CO_2$ assimilation (from −16% to −28% at a PFD ≥ 140 μmol $m^{-2}$ $s^{-1}$; $P \leq 0.04$; Fig. 4a). The strong reduction in stomatal conductance in relation to the moderate reduction in $CO_2$ assimilation resulted in a strong increase in intrinsic water-use efficiency (¡WUE) particularly in low light (from 68% to 94% at a PFD ≤ 140 μmol $m^{-2}$ $s^{-1}$; $P \leq 0.006$). Similar to *psi3-1*, the *psi3-2* mutant differed from the WT in NPQ and photosynthetic parameters, but to a lesser extent. At fluctuating, light mutants showed a similar response as at steady-state light conditions (Fig. S21). To assess whether the differences in $A_n$ were solely the result of differences in stomatal conductance, $CO_2$ response curves were quantified (Fig. 4e). At ambient as well as at saturated $CO_2$ concentrations, the intercellular $CO_2$ concentration in mutants' leaves was the same if not higher than in WT. Mutants showed significantly lower $J$ (from 15% to 22%, $P = 0.002$), and TPU (from 17% to 23%, $P = 0.004$) and a nonsignificantly reduction in $V_{cmax}$ (11.5%, $P = 0.3$), compared with WT (Fig. 4e). The pattern of difference in light response curves between *PSI3* mutants and wild-type plants remained consistent even in plants grown at elevated $CO_2$ concentrations (Fig. S22). While NPQ was still affected in mutants, the differences were somewhat less pronounced as a result of a general reduction in NPQ observed in all three investigated lines when grown under elevated $CO_2$.

## Discussion

Here, we quantified numerous traits describing distinct attributes of NPQ and ΦPSII kinetics in a genetically diverse panel of maize genotypes in light and dark conditions. We collected leaf disks from field-grown plants and subjected them to a light period followed by a dark adaptation to measure changes in chlorophyll fluorescence. The large number of simultaneously measured disks enabled by this approach allowed us to phenotype, on average, 671 disks per day, generating detailed and semi-high-throughput data on NPQ and ΦPSII kinetics. Despite the use of detached leaf tissue our measured $F_v/F_m$, NPQ and ΦPSII values were similar to those recorded on maize plants grown in a growth chamber (Bashir *et al.*, 2021) and a field (Meena *et al.*, 2021) and we successfully reidentified the maize copy of *PSBS* (Figs 1c, 2a, S16); a known genetic factor associated with variation in NPQ function across a number of experiments (Li *et al.*, 2000; Kasajima *et al.*, 2011; Herritt *et al.*, 2016; Wang *et al.*, 2017; Rungrat *et al.*, 2019). In addition, we detected many more significant marker–trait associations across the genome than previous studies of NPQ and/or ΦPSII. In field-grown rice, 33 loci with nine candidate genes of known functions were significantly associated with NPQ (Wang *et al.*, 2017). In sorghum (*Sorghum bicolor*) grown under control conditions, 12 SNPs with 10 candidate genes were significantly associated with ΦPSII (Ortiz *et al.*, 2017). Herritt *et al.* (2016) reported 28 candidate genes significantly associated with NPQ in soybean (*Glycine max*) using the photochemical reflectance index to approximate NPQ. This difference may be explained by capturing more types of variation in NPQ and ΦPSII (e.g. both rates of change and steady-state values), by differences in statistical approaches employed for GWAS, or simply by the greater statistical power provided by the use of a larger association panel.

The single most significant signal in our study originated from a SNP located in a maize gene encoding an uncharacterized protein, which we identified as an ortholog of Arabidopsis *PSI3*. The SNP identified by GWAS in maize is in high linkage disequilibrium (0.93) with a SNP altering a threonine to an isoleucine within the coding sequence of *PSI3*. Previous efforts to functionally characterize this protein in Arabidopsis suggest it may play a fundamental role in plant growth and regulation of carbon metabolism (Stührwohldt *et al.*, 2014). Plants lacking functional PSI3 exhibit reduced cell growth, altered stomatal patterning, and retarded shoot growth. By contrast, *PSI3* overexpression promotes plant growth.

Here, we showed that loss of PSI3 function in Arabidopsis strongly and negatively affected NPQ in light and dark conditions (Figs 3e,h,j–l, S19c,d,g,h,m). Interestingly, two traits particularly important for photosynthetic efficiency in fluctuating light (i.e. the rate of ΦPSII recovery and the ratio of ΦPSII recovery to the NPQ residual at the end of the dark period) were significantly higher in the *psi3-1* mutant by 25% and 28%, respectively, relative to the WT (Fig. S20h,l). These differences in ΦPSII cannot be simply explained by impairment of NPQ because we did not observe a similar ΦPSII phenotype in, for example, the *irm1* mutant, which otherwise exhibited NPQ kinetics similar to those observed in *psi3-1*. Examining NPQ at different light intensities revealed that PSI3 regulated NPQ in a light-dosage-dependent manner (Fig. 4a,c,d) that may be partially explained by the presence of a DUF668 domain in both the maize and Arabidopsis *PSI3* genes (Stührwohldt *et al.*, 2014). Genes encoding the DUF668 domain are highly regulated by light through their *cis*-regulatory elements (Zhong *et al.*, 2019). A large reduction in net $CO_2$ assimilation in the *psi3* mutants might, at least partly, result from a substantial reduction in stomatal conductance (Fig. 4). However, data from $CO_2$ responsive curves, as well as from plants grown under elevated $CO_2$ conditions, demonstrated that the lower $A_n$ of *psi3* mutants is not the result of reduced $C_i$ in mutant leaves but rather to limitation in linear electron transport and triose phosphate utilization rates (Figs 4e, S22).

Two of the five additional genes linked to GWAS hits in maize and NPQ and/or ΦPSII phenotypes when knocked out in Arabidopsis are thioredoxins (*TRX-Y1* and *ACHT3*). Two enzymes contributing to NPQ, *VDE*, and *ZEP*, are direct thioredoxin targets (Hall *et al.*, 2010; Da *et al.*, 2018), and thioredoxin-mediated systems may also influence NPQ independently of light-induced changes in proton gradient across the thylakoid membrane (Nikkanen *et al.*, 2019). A third, *PMI1*, encodes a plant-specific protein whose light-induced displacement initiates blue-light-induced chloroplast movement (DeBlasio *et al.*, 2005; Dwyer & Hangarter, 2022). Chloroplast movement away from strong light contributes to photoprotection together with NPQ. Therefore, these two mechanisms might interplay to modulate PSII efficiency and optimize light utilization.

The high-rate genes identified as candidates in maize exhibited in NPQ and/or ΦPSII defects when disrupted in Arabidopsis is

striking. The lineages leading to these two species are estimated to have diverged from each other 160 million years ago (Kumar *et al.*, 2017), and the candidate genes were identified in a species utilizing $C_4$ photosynthesis and evaluated in a species utilizing $C_3$ photosynthesis. Both the lengthy evolutionary divergence and the difference in photosynthetic system employed by these two species increased the risk of false-negative validation in Arabidopsis (e.g. identifying genes which genuinely do play a role in controlling variation in NPQ-related traits in maize, yet failing to replicate the phenotype in Arabidopsis because the role is either $C_4$ specific, the gene gained NPQ-related function on the lineage leading to maize, or the gene lost NPQ related function on the lineage leading to Arabidopsis). However, neither of these issues should significantly increase the risk of false-positive associations. The substantial number of cases where knockout alleles of the Arabidopsis orthologs of maize candidate genes did indeed influence NPQ is consistent with a high degree of conservation of NPQ across evolutionary time and photosynthetic innovations. An additional concern is that loss of function mutations of the type used in Arabidopsis in this study are likely to be more severe than naturally segregating variants in a population. Large effect mutations could influence photosynthesis and NPQ indirectly via effects on plant growth and vigor and produce false positives in our effort to validate maize candidate genes. However, one observation that mitigates this concern is that in four out of six cases (*PSI3*, *TRX-Y1*, *ACHT3*, and *IRM1*) not only did loss of function mutants in the Arabidopsis orthologs of maize candidate also exhibit altered NPQ and/or ΦPSII kinetics, but these mutants exhibited the same specific kinds of kinetic changes observed in the naturally occurring maize variants.

In this work, we employed a semi-high-throughput phenotyping method to conduct a GWAS on a diverse maize panel grown in the field to identify a set of trait-associated SNPs and linked candidate genes controlling natural variation in NPQ and ΦPSII kinetics. Out of the six maize candidate genes we investigated, all six knockout mutants of their orthologs in Arabidopsis exhibited significant differences in NPQ and/or ΦPSII relative to the WT. Identifying here genes and naturally occurring variant alleles involved in NPQ and ΦPSII kinetics considerably expands the toolbox for engineering plants to optimize photosynthesis and improve yield in field-grown crops.

## Acknowledgements

We thank Christine Smith for managing the field experiments, Jill Belgen, Quinton Browne, Rachel Gerdes, Quinn Kimbell, Bailey McLean, and Annie Nelson for assistance during field data collection, and Cailin Smith for assistance in data extraction from fluorescence images. This research was supported by the National Science Foundation under award no. OIA-1557417 for the Center for Root and Rhizobiome Innovation (CRRI), by the US Department of Energy, Grant no. DE-SC0020355, USDA-NIFA under the AI Institute: for Resilient Agriculture, Award no. 2021-67021-35329 and by Foundation for Food and Agriculture Research Award no. 602757. KG was supported by the National Science Foundation supporting Nebraska Established Program to Stimulate Competitive Research program under FIRST Award, Layman Fund held at the University of Nebraska Foundation and National Science Foundation CAREER grant no. 2142993.

## Competing interests

None declared.

## Author contributions

SS, MG, JCS and KG designed the experiments. SS and MG performed the experiments and data analyses. SS, MG, JCS and KG wrote the manuscript. SS and MG contributed equally to this work.

## ORCID

Katarzyna Głowacka https://orcid.org/0000-0002-8892-1482
Marcin Grzybowski https://orcid.org/0000-0002-6303-5433
Seema Sahay https://orcid.org/0000-0001-5707-2206
James C. Schnable https://orcid.org/0000-0001-6739-5527

## Data availability

Supporting Figures, Tables, Methods, and Datasets corresponding to the figures and results described in this manuscript may be found online in the Supporting Information section. Custom code and scripts written to conduct analyses described in this paper are provided in a github repository associated with this paper: https://github.com/mgrzy/Maize_NPQ_Natural_Variation.

## References

**Alonso JM, Stepanova AN, Leisse TJ, Kim CJ, Chen H, Shinn P, Stevenson DK, Zimmerman J, Barajas P, Cheuk R. 2003.** Genome-wide insertional mutagenesis of *Arabidopsis thaliana*. *Science* **301**: 653–657.

**Bashir N, Athar HU, Kalaji HM, Wróbel J, Mahmood S, Zafar ZU, Ashraf M. 2021.** Is photoprotection of PSII one of the key mechanisms for drought tolerance in maize? *International Journal of Molecular Sciences* **22**: 13490.

**Bates D, Mächler M, Bolker B, Walker S. 2015.** Fitting linear mixed-effects models using LME4. *Journal of Statistical Software* **67**: i01.

**Bilger W, Björkman O. 1994.** Relationships among violaxanthin deepoxidation, thylakoid membrane conformation, and nonphotochemical chlorophyll fluorescence quenching in leaves of cotton (*Gossypium hirsutum* L.). *Planta* **193**: 238–246.

**Burgess AJ, Retkute R, Preston SP, Jensen OE, Pound MP, Pridmore TP, Murchie EH. 2016.** The 4-dimensional plant: effects of wind-induced canopy movement on light fluctuations and photosynthesis. *Frontiers in Plant Science* **7**: 1392.

**Chibani K, Pucker B, Dietz KJ, Cavanagh A. 2021.** Genome-wide analysis and transcriptional regulation of the typical and atypical thioredoxins in *Arabidopsis thaliana*. *FEBS Letters* **595**: 2715–2730.

**Cingolani P, Platts A, Wang le L, Coon M, Nguyen T, Wang L, Land SJ, Lu X, Ruden DM. 2012.** A program for annotating and predicting the effects of single nucleotide polymorphisms, SnpEff: SNPs in the genome of *Drosophila melanogaster* strain w1118; iso-2; iso-3. *Fly* **6**: 80–92.

**Da Q, Sun T, Wang M, Jin H, Li M, Feng D, Wang J, Wang HB, Liu B. 2018.** M-type thioredoxins are involved in the xanthophyll cycle and proton motive force to alter NPQ under low-light conditions in Arabidopsis. *Plant Cell Reports* **37**: 279–291.

**Dalin C, Wada Y, Kastner T, Puma MJ. 2017.** Groundwater depletion embedded in international food trade. *Nature* **543**: 700–704.

**Dangoor I, Peled-Zehavi H, Levitan A, Pasand O, Danon AA. 2009.** Small family of chloroplast atypical thioredoxins. *Plant Physiology* **149**: 1240–1250.

**De Souza AP, Burgess SJ, Doran L, Hansen J, Manukyan L, Maryn N, Gotarkar D, Leonelli L, Niyogi KK, Long SP. 2022.** Soybean photosynthesis and crop yield are improved by accelerating recovery from photoprotection. *Science* **377**: 851–854.

**DeBlasio SL, Luesse DL, Hangarter RPA. 2005.** plant-specific protein essential for blue-light-induced chloroplast movements. *Plant Physiology* **139**: 101–114.

**Demmig-Adams B. 1990.** Carotenoids and photoprotection in plants: a role for the xanthophyll zeaxanthin. *Biochimica et Biophysica Acta* **1020**: 1–24.

**Demmig-Adams B, Koh S-C, Cohu CM, Muller O, Stewart JJ, Adams WW III. 2014.** Non-photochemical fluorescence quenching in contrasting plant species and environments. In: Demmig-Adams B, Garab G, Adams WW III, Govindjee, eds. *Non-photochemical quenching and energy dissipation in plants, algae and cyanobacteria*. Dordrecht, the Netherlands: Springer, 531–552.

**Dwyer ME, Hangarter RP. 2022.** Light-induced displacement of PLASTID MOVEMENT IMPAIRED1 precedes light-dependent chloroplast movements. *Plant Physiology* **189**: 1866–1880.

**Farquhar GD, Von CS, Berry J. 1980.** A biochemical model of photosynthesis $CO_2$ fixation in leaves of C3 species. *Planta* **149**: 78–90.

**Ferro M, Salvi D, Riviere-Rolland H, Vermat T, Seigneurin-Berny D, Grunwald D, Garin J, Joyard J, Rolland N. 2002.** Integral membrane proteins of the chloroplast envelope: identification and subcellular localization of new transporters. *Proceedings of the National Academy of Sciences, USA* **99**: 11487–11492.

**Gage JL, Vaillancourt B, Hamilton JP, Manrique-Carpintero NC, Gustafson TJ, Barry K, Lipzen A, Tracy WF, Mikel MA, Kaeppler SM *et al.* 2019.** Multiple maize reference genomes impact the identification of variants by genome-wide association study in a diverse inbred panel. *The Plant Genome* **12**: 180069.

**Genty B, Briantais JM, Baker NR. 1989.** The relationship between the quantum yield of photosynthetic electron transport and quenching of chlorophyll fluorescence. *Biochimica et Biophysica Acta* **990**: 87–92.

**Goetze TA, Philippar K, Ilkavets I, Soll J, Wagner R. 2006.** OEP37 is a new member of the chloroplast outer membrane ion channels. *Journal of Biological Chemistry* **281**: 17989–17998.

**Grzybowski M, Mural RV, Xu G, Turkus J, Jinliang Y, Schnable JC. 2023.** A common resequencing-based genetic marker dataset for global maize diversity. *The Plant Journal* **113**: 1109–1121.

**Hall M, Mata-Cabana A, Akerlund HE, Florencio FJ, Schröder WP, Lindahl M, Kieselbach T. 2010.** Thioredoxin targets of the plant chloroplast lumen and their implications for plastid function. *Proteomics* **10**: 987–1001.

**Hansey CN, Johnson JM, Sekhon RS, Kaeppler SM, de Leon N. 2011.** Genetic diversity of a maize association population with restricted phenology. *Crop Science* **51**: 704–715.

**Herritt M, Dhanapal AP, Fritschi FB. 2016.** Identification of genomic loci associated with the photochemical reflectance index by genome-wide association study in soybean. *Plant Genome* **9**: plantgenome2015.08.0072.

**Hirsch CN, Foerster JM, Johnson JM, Sekhon RS, Mutton G, Vaillancourt B, Peñagaricano F, Lindquist E, Pedraza MA, Barry K *et al.* 2014.** Insights into the maize pan-genome and pan-transcriptome. *Plant Cell* **26**: 121–135.

**Hubbart S, Ajigboye OO, Horton P, Murchie EH. 2012.** The photoprotective protein PsbS exerts control over $CO_2$ assimilation rate in fluctuating light in rice. *The Plant Journal* **71**: 402–412.

**Jung HS, Niyogi KK. 2009.** Quantitative genetic analysis of thermal dissipation in Arabidopsis. *Plant Physiology* **150**: 977–986.

**Kasajima I, Ebana K, Yamamoto T, Takahara K, Yano M, Kawai-Yamada M, Uchimiya H. 2011.** Molecular distinction in genetic regulation of nonphotochemical quenching in rice. *Proceedings of the National Academy of Sciences, USA* **108**: 13835–13840.

**Kim JS, Kug J-S, Jeong S-J, Huntzinger DN, Michalak AM, Schwalm CR, Wei Y, Schaefer K. 2017.** Reduced North American terrestrial primary productivity linked to anomalous Arctic warming. *Nature Geoscience* **10**: 572–576.

**Köhler IH, Ruiz-Vera UM, VanLoocke A, Thomey ML, Clemente T, Long SP, Ort DR, Bernacchi CJ. 2017.** Expression of cyanobacterial FBP/SBPase in soybean prevents yield depression under future climate conditions. *Journal of Experimental Botany* **68**: 715–726.

**Kromdijk J, Głowacka K, Leonelli L, Gabilly ST, Iwai M, Niyogi KK, Long SP. 2016.** Improving photosynthesis and crop productivity by accelerating recovery from photoprotection. *Science* **354**: 857–861.

**Kumar S, Stecher G, Suleski M, Hedges SB. 2017.** TimeTree: a resource for timelines, timetrees, and divergence times. *Molecular Biology and Evolution* **34**: 1812–1819.

**Li XP, Björkman O, Shih C, Grossman AR, Rosenquist M, Jansson S, Niyogi KK. 2000.** A pigment-binding protein essential for regulation of photosynthetic light harvesting. *Nature* **403**: 391–395.

**Liu X, Huang M, Fan B, Buckler ES, Zhang Z. 2016.** Iterative usage of fixed and random effect models for powerful and efficient genome-wide association studies. *PLoS Genetics* **12**: e1005767.

**Lobell DB, Roberts MJ, Schlenker W, Braun N, Little BB, Rejesus RM, Hammer GL. 2014.** Greater sensitivity to drought accompanies maize yield increase in the U.S. midwest. *Science* **344**: 516–519.

**Long SP, Bernacchi CJ. 2003.** Gas exchange measurements, what can they tell us about the underlying limitations to photosynthesis? Procedures and sources of error. *Journal of Experimental Botany* **54**: 2393–2401.

**López-Calcagno PE, Brown KL, Simkin AJ, Fisk SJ, Vialet-Chabrand S, Lawson T, Raines CA. 2020.** Stimulating photosynthetic processes increases productivity and water-use efficiency in the field. *Nature Plants* **6**: 1054–1063.

**Loriaux SD, Avenson TJ, Welles JM, McDermitt DK, Eckles RD, Riensche B, Genty B. 2013.** Closing in on maximum yield of chlorophyll fluorescence using a single multiphase flash of sub-saturating intensity. *Plant, Cell & Environment* **36**: 1755–1770.

**Mazaheri M, Heckwolf M, Vaillancourt B, Gage JL, Burdo B, Heckwolf S, Barry K, Lipzen A, Ribeiro CB, Kono TJY. 2019.** Genome-wide association analysis of stalk biomass and anatomical traits in maize. *BMC Plant Biology* **19**: 45.

**Meena R, Reddy KS, Gautam R, Maddela S, Reddy AR, Gudipalli P. 2021.** Improved photosynthetic characteristics correlated with enhanced biomass in a heterotic F1 hybrid of maize (*Zea mays* L.). *Photosynthesis Research* **147**: 253–267.

**Müller P, Li XP, Niyogi KK. 2001.** Non-photochemical quenching. A response to excess light energy. *Plant Physiology* **125**: 1558–1566.

**Mural RV, Sun G, Grzybowski M, Tross MC, Jin H, Smith C, Newton L, Andorf CM, Woodhouse MR, Thompson AM *et al.* 2022.** Association mapping across a multitude of traits collected in diverse environments identifies pleiotropic loci in maize. *Gigascience* **11**: giac080.

**Nikkanen L, Guinea Diaz M, Toivola J, Tiwari A, Rintamäki E. 2019.** Multilevel regulation of non-photochemical quenching and state transitions by chloroplast NADPH-dependent thioredoxin reductase. *Plant Physiology* **166**: 211–225.

**Oakley CG, Savage L, Lotz S, Larson GR, Thomashow MF, Kramer DM, Schemske DW. 2018.** Genetic basis of photosynthetic responses to cold in two locally adapted populations of *Arabidopsis thaliana*. *Journal of Experimental Botany* **69**: 699–709.

**Ortiz D, Hu J, Salas Fernandez MG. 2017.** Genetic architecture of photosynthesis in *Sorghum bicolor* under non-stress and cold stress conditions. *Journal of Experimental Botany* **68**: 4545–4557.

**Purcell S, Neale B, Todd-Brown K, Thomas L, Ferreira MA, Bender D, Maller J, Sklar P, de Bakker PI, Daly MJ *et al.* 2007.** Plink: a tool set for whole-genome association and population-based linkage analyses. *American Journal of Human Genetics* **81**: 559–575.

**Ray DK, Ramankutty N, Mueller ND, West PC, Foley JA. 2012.** Recent patterns of crop yield growth and stagnation. *Nature Communications* **3**: 1293.

**Roach T, Krieger-Liszkay A. 2012.** The role of the PsbS protein in the protection of photosystems I and II against high light in *Arabidopsis thaliana*. *Biochimica et Biophysica Acta* **1817**: 2158–2165.

**Ruban AV, Wilson S. 2021.** The mechanism of non-photochemical quenching in plants: localization and driving forces. *Plant and Cell Physiology* **62**: 1063–1072.

**Rungrat T, Almonte AA, Cheng R, Gollan PJ, Stuart T, Aro E-M, Borevitz JO, Pogson B, Wilson PB. 2019.** A genome-wide association study of non-photochemical quenching in response to local seasonal climates in *Arabidopsis thaliana*. *Plant Direct* **3**: e00138.

**Sharkey TD, Bernacchi CJ, Farquhar GD, Singsaas EL. 2007.** Fitting photosynthetic carbon dioxide response curves for $C_3$ leaves. *Plant, Cell & Environment* **30**: 1035–1040.

**South PF, Cavanagh AP, Liu HW, Ort DR. 2019.** Synthetic glycolate metabolism pathways stimulate crop growth and productivity in the field. *Science* **363**: eaat9077.

**Stührwohldt N, Hartmann J, Dahlke RI, Oecking C, Sauter M. 2014.** The PSI family of nuclear proteins is required for growth in arabidopsis. *Plant Molecular Biology* **86**: 289–302.

**Valdar W, Holmes CC, Mott R, Flint J. 2009.** Mapping in structured populations by resample model averaging. *Genetics* **182**: 1263–1277.

**Vanacker H, Guichard M, Bohrer AS, Issakidis-Bourguet E. 2018.** Redox regulation of monodehydroascorbate reductase by thioredoxin y in plastids revealed in the context of water stress. *Antioxidants* **7**: 183.

**Wang Q, Zhao H, Jiang J, Xu J, Xie W, Fu X, Liu C, He Y, Wang G. 2017.** Genetic architecture of natural variation in rice nonphotochemical quenching capacity revealed by genome-wide association study. *Frontiers in Plant Science* **8**: 1773.

**Yamamoto HY, Nakayama TOM, Chichester CO. 1962.** Studies on the light and dark interconversions of leaf xanthophylls. *Archives of Biochemistry and Biophysics* **97**: 168–173.

**Yin L, Zhang H, Tang Z, Xu J, Yin D, Zhang Z, Yuan X, Zhu M, Zhao S, Li X. 2021.** rMVP: a memory-efficient, visualization-enhanced, and parallel-accelerated tool for genome-wide association study. *Genomics, Proteomics & Bioinformatics* **19**: 619–628.

**Yu J, Pressoir G, Briggs WH, Vroh Bi I, Yamasaki M, Doebley JF, McMullen MD, Gaut BS, Nielsen DM, Holland JB *et al.* 2006.** A unified mixed-model method for association mapping that accounts for multiple levels of relatedness. *Nature Genetics* **38**: 203–208.

**Zhao C, Liu B, Piao S, Wang X, Lobell DB, Huang Y, Huang M, Yao Y, Bassu S, Ciais P *et al.* 2017.** Temperature increase reduces global yields of major crops in four independent estimates. *Proceedings of the National Academy of Sciences, USA* **114**: 9326–9331.

**Zhong H, Zhang H, Guo R, Wang Q, Huang X, Liao J, Li Y, Huang Y, Wang Z. 2019.** Characterization and functional divergence of a novel *DUF668* gene family in rice based on comprehensive expression patterns. *Genes* **10**: 980.

**Zhu X, Ort DR, Whitmarsh J, Long SP. 2004.** The slow reversibility of photosystem II thermal energy dissipation on transfer from high to low light may cause large losses in carbon gain by crop canopies: A theoretical analysis. *Journal of Experimental Botany* **55**: 1167–1175.

## Supporting Information

Additional Supporting Information may be found online in the Supporting Information section at the end of the article.

**Dataset S1** Data collected from the fluorescence assay for 751 maize genotypes in the 2020 field season.

**Dataset S2** Data collected from the fluorescence assay for 782 maize genotypes in the 2021 field season.

**Dataset S3** Data collected from the fluorescence assay for seven Arabidopsis T-DNA insertional mutants and wild-type grown in the growth chamber.

**Dataset S4** Steady state photosynthesis-related parameters as a function of light in wild-type Arabidopsis and two *psi3* mutants.

**Dataset S5** Photosynthesis-related parameters as a function of incident photon flux density under fluctuating light in wild-type Arabidopsis and two *psi3* mutants.

**Dataset S6** Photosynthesis-related parameters as a function of intercellular $CO_2$ concentration in wild-type Arabidopsis and two psi3 mutants.

**Dataset S7** Steady-state response of photosynthetic parameters as a function of light for high-$CO_2$-grown wild-type Arabidopsis and two psi3 mutants.

**Fig. S1** Weather conditions during the field experiments in 2020 and 2021.

**Fig. S2** Schematic representation of the putative location of the T-DNA insertion in the Arabidopsis mutants.

**Fig. S3** Light intensities used to measure the response of photosynthesis-related parameters to steady state or fluctuating light in the Arabidopsis *psi3* mutants and the corresponding wild-type.

**Fig. S4** Distribution of kinetics curves of nonphotochemical quenching (NPQ) and photosystem II operating efficiency (ΦPSII) observed from leaf disk-phenotyping of maize in two field seasons.

**Fig. S5** Distribution of Pearson's correlation between maize NPQ and ΦPSII traits measured in the 2020 field study and maize hand-measured plant traits.

**Fig. S6** Transcriptome-wide association studies for NPQ traits in maize.

**Fig. S7** Genomic intervals, neighboring genes, and nonsynonymous mutations associated with the five maize candidate genes evaluated in this study.

**Fig. S8** Expression GWAS conducted for the six candidate maize genes evaluated in this study.

**Fig. S9** Relationship between NPQ and ΦPSII traits observed for the same maize diversity panel in 2 yr.

**Fig. S10** Consistent effects of SNP Chr3:176152936 in maize across 2 yr.

**Fig. S11** Consistent effects of SNP Chr2:182382835 in maize across 2 yr.

**Fig. S12** Consistent effects of SNP Chr3:147531265 in maize across 2 yr.

**Fig. S13** Consistent effects of SNP Chr7:179281748 in maize across 2 yr.

**Fig. S14** Consistent effects of SNP Chr1:86064177 in maize across 2 yr.

**Fig. S15** Effects of SNP Chr5:187859720 in maize across 2 yr.

**Fig. S16** Resampling-based GWAS conducted for 25 NPQ- and ΦPSII-related traits measured in maize during the 2021 field season.

**Fig. S17** Verification of homozygosity in the Arabidopsis T-DNA insertional mutant *acht3*, *irm1*, *oep37*, *pmi1*, *psi3-1*, *psi3-2*, and *trx-y1*.

**Fig. S18** Verification of the absence of mature transcripts of *ACHT3*, *IRM1*, *OEP37*, *PMI1*, *PSI3*, and *TRX-Y1* in the Arabidopsis T-DNA insertional mutants.

**Fig. S19** Genotypic variation for the 13 NPQ, ΦPSII, and $F_v/F_m$ traits in the Arabidopsis T-DNA insertional mutants.

**Fig. S20** Validation of six candidate genes in the Arabidopsis T-DNA insertional mutants based on six ΦPSII traits.

**Fig. S21** Response of photosynthesis-related parameters to fluctuating light conditions in Arabidopsis wild-type (WT) plants and the *psi3-1* and *psi3-2* mutants.

**Fig. S22** Response of photosynthesis-related parameters to gradual changes in light conditions in Arabidopsis wild-type (WT) plants and the *psi3-1* and *psi3-2* mutants grown under high-$CO_2$ conditions.

**Methods S1** Maize field design, establishment, and management.

**Methods S2** PCR and RT-PCR.

**Table S1** List of the 804 maize genotypes used in the field study.

**Table S2** Schematic representations of the maize field experimental design in 2020.

**Table S3** Schematic representations of the maize field experimental design in 2021.

**Table S4** Abbreviations, full names, and descriptions of NPQ and ΦPSII traits investigated in this study.

**Table S5** Primer sequences used for PCR and RT-PCR to verify the Arabidopsis T-DNA insertional mutants.

**Table S6** List of SNPs associated with NPQ and ΦPSII traits and the maize candidate genes localized within 10 kb of each SNP for the 2020 field season.

**Table S7** List of candidate maize genes localized within 10 kb of SNPs associated with NPQ and ΦPSII traits for the 2020 field season.

**Table S8** Maize allelic variation for *PSBS*, known to influence NPQ, and six candidate genes significantly associated with NPQ and ΦPSII traits.

**Table S9** List of nonsynonymous mutations in maize candidate genes and linkage disequilibrium with the associated maize GWAS hit.

**Table S10** List of SNPs associated with NPQ and ΦPSII traits and the maize candidate genes localized within 10 kb of each SNP for the 2021 field season.

**Table S11** List of candidate maize genes localized within 10 kb of SNPs associated with NPQ and ΦPSII traits for the 2021 field season.

Please note: Wiley is not responsible for the content or functionality of any Supporting Information supplied by the authors. Any queries (other than missing material) should be directed to the *New Phytologist* Central Office.